Int. J. Electrochem. Sci., 15**(2020)** 1160 – 1168, doi: 10.20964/2020.02.09

International Journal of
ELECTROCHEMICAL
SCIENCE
www.electrochemsci.org

One-Step Electrochemical Synthesis and Assembly of MnO_2/Graphene and its Application for Supercapacitors

Xin Cao[1,], Liguo Ma[2], Aiqin Tian[1], Hanlin Zhang[1], Maojun Zheng[2,4], Shaohua Liu[3*], Qiang Li[2], Yuxiu You[2], Faze Wang[2], Li Ma[5] and Wenzhong Shen[2]*

[1] National Engineering Research Center for High-Speed EMU, China Railway Rolling Stock (CRRC) Qingdao Si Fang Co., LTD., Qingdao, 266111, PR China
[2] Key Laboratory of Artificial Structure and Quantum Control, Ministry of Education, Department of Physics and Astronomy, Shanghai Jiao Tong University, Shanghai, 200240, PR China
[3] State Key Laboratory of Precision Spectroscopy & School of Physics and Materials Science, East China Normal University, 200241, PR China
[4] Collaborative Innovation Center of Advanced Microstructures, Nanjing University, Nanjing, 210093, PR China
[5] School of Chemistry and Chemical Technology, Shanghai Jiao Tong University, Shanghai, 200240, PR China
[*]E-mail: doudoucao@163.com (X. Cao)

Received: 19 June 2019 / *Accepted:* 7 August 2019 / *Published:* 31 December 2019

We developed a facile, rapid, scalable, and environmentally friendly route to synchronously achieve ultrathin, high-quality graphene and MnO_2 nanosheets, which spontaneously migrated and coassembled on a cathodic 3D Ni foam. The resultant 3D MnO_2/graphene electrodes exhibited excellent performance for a supercapacitor in terms of capacitance, rate capability and cycle life.

Keywords: Two-dimensional Nanosheet; Self-assembly; Graphene; MnO_2; Superconductors

1. INTRODUCTION

Currently, supercapacitors as a promising energy source have been extensively studied [1-6]. Their performance depends to a large extent on the type and microstructure of the electrode materials, including power density and energy density. As a supercapacitor electrode material, MnO_2 exhibited exceptional competitiveness due to its abundance, environmental friendliness and very high theoretical capacitance (1232 F g^{-1}) [7, 8]. However, drawbacks in the conductivity and stability of MnO_2 limit its practical applications for supercapacitors.

The hybridization of MnO_2 electrodes with conducting carbon materials has been demonstrated to be a good strategy to address its problems. In this way, carbon nanotubes[9], activated carbon[10] and graphene[11-15], have been explored for the fabrication of MnO_2-based supercapacitors. For instance, Qian fabricated 3D porous graphene-MnO_2 composites by depositing MnO_2 particles on graphene by freeze-drying, and these composites achieved a high capacitance of 258 F g^{-1}[16]. Peng developed quasi-2D MnO_2/graphene nanosheets used for in-plane supercapacitors with a capacitance of 267 F g^{-1}[17]. Despite great progress, the fabrication of MnO_2/graphene electrodes often suffer from a multistep, complicated and costly procedure; thus, the development of new fabrication approaches for high-performance MnO_2-based hybrid electrode materials is urgently needed.

Herein, we propose a facile strategy to prepare a MnO_2/graphene composite electrode *via* an electrochemically assisted route. High-quality conductive graphene was exfoliated from anodic graphite and accompanied with the growth of ultrathin MnO_2 nanosheets from an electrolyte solution. Following that, the electrochemically exfoliated graphene and ultrathin MnO_2 nanosheets simultaneously rapidly migrated and spontaneously assembled on the cathodic 3D Ni foam. The resultant 3D MnO_2/graphene electrodes achieved excellent capacitance (607 F g^{-1} at 1 A g^{-1}), high rate capability and super cycling stability (94.1 % after 10000 charge-discharge cycles).

2. EXPERIMENTAL

2.1 Synthesis of MnO_2/graphene composites.

The MnO_2/graphene composites were synthesized using a unique electrochemical technique that is simple, green and inexpensive. In a typical synthesis, we performed a two-electrode system using graphite flakes as the anode and Ni foam as the cathode (both with a working area of approximately 2.0*1.0 cm^2), and the electrolyte was a mixed aqueous solution containing 20 mg $KMnO_4$ and 100 mL 0.1 M Na_2SO_4. When a direct current voltage of 10 V was applied to the two-electrode setup, vigorous bubbles were produced at the electrodes, and anodic graphite began to dissociate into graphene sheets, which were dispersed into the electrolyte. Meanwhile, MnO_4^- was reduced to MnO_2 on the surface of the cathodic Ni foam. The reaction took place at 25 °C for 30 min. Then, the MnO_2/graphene composites were washed three times with H_2O and dried at 60 °C for 12 h.

2.2 Electrochemical Measurements.

The electrochemical properties were performed using a PARSTAT 4000 workstation (Princeton Applied Research, Ametek, USA) with a standard three-electrode system. Using the prepared samples as the working electrodes with a Pt clamp, a Pt gauze as the counter electrode, and a saturated calomel reference electrode. Cyclic voltammetry with various scan rates between 0.0 and 0.8 V was conducted in 1 M Na_2SO_4. The galvanostatic charge-discharge measurements (GCD) and cycle stability were performed on a LAND CT-2001A.

2.3 Characterization

The morphology of the MnO_2/graphene composite was observed by SEM (JEOL JSM-7401F) with an accelerating voltage of 1.0 kV. To understand the surface information of the as-synthesized samples, XPS (AXIS ULTRA DLD, Kratos, Japan) was conducted to analyze the composition of the sample surface. The Raman spectra were obtained using a laser micro-Raman spectrometer (Renishaw inVia) employing an argon-ion laser with an incident wavelength of 532 nm.

3. RESULTS AND DISCUSSION

our previous study demonstrated that high-quality graphene can be directly exfoliated from graphite and self-assembled on a cathodic Ni foam with the assistance of an electric field, which makes it possible for one-step growth and coassembly of electrochemical exfoliated graphene and ultrathin MnO_2 nanosheets on the cathodic surfaces. [18] As shown in Figure 1, electrochemical exfoliation of graphite was conducted in a two-electrode reaction system in which graphite flakes and Ni foam worked as an anode and cathode, respectively. Electrolyte was prepared by mixing 100 ml of 0.1 M Na_2SO_4 and 20 mg $KMnO_4$. Under a direct current voltage of 10 V, the graphite gradually dissociated and dispersed into the electrolyte. The exfoliated graphene sheets were investigated by SEM and TEM (Fig. 2), which clearly demonstrates the formation of high-quality, few-layer graphene nanosheets. Despite the high quality of the graphene, the resulting graphene derived from an electrochemical-assisted exfoliation still possessed negative charges at their edges, which would prompt their assembly on the Ni foam surfaces due to electrostatic interactions. Meanwhile, MnO_4^- was reduced to MnO_2 nanosheets by the following reaction (1), and these sheets spontaneously assembled on the Ni foam surface under an electric field. Therefore, the hybrid MnO_2/graphene composites on 3D Ni foam can be obtained via one-step growth and coassembly resulting in high-quality EG and ultrathin MnO_2 nanosheets.

$$MnO_4^- + 2H_2O + 3\,e^- \longrightarrow MnO_2 + 4OH^- \qquad (1)$$

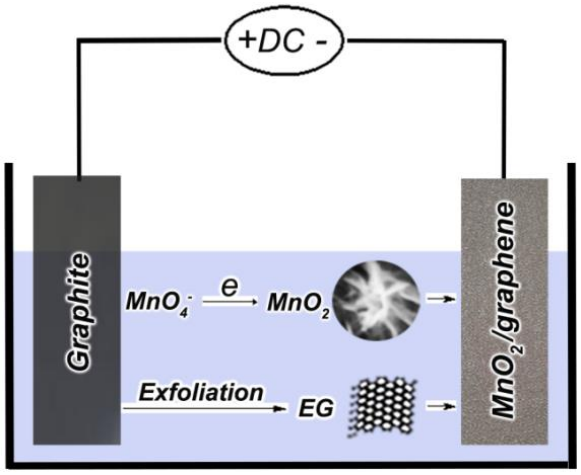

Figure 1. Schematic illustration of one-step electrochemical preparation of exfoliated graphene and ultrathin MnO_2 nanosheets with their coassembly on 3D Ni foam electrodes.

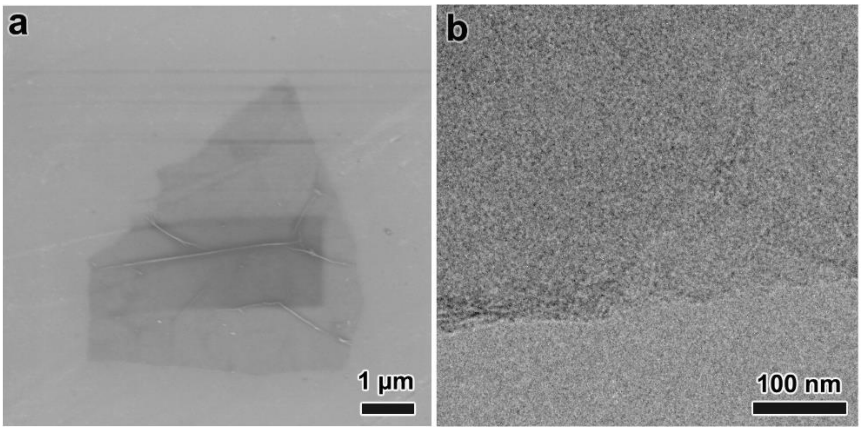

Figure 2. SEM (a) and TEM (b) images of the exfoliated graphene nanosheets.

The structure of the MnO_2/graphene composites was characterized by Raman spectroscopy (Fig. 3a). The Raman spectrum of the MnO_2/graphene composites presents three obvious, characteristic vibration bands at 1350 cm^{-1}, 1583 cm^{-1} and 2700 cm^{-1}, corresponding to the D, G and 2D bands of graphene, respectively. In addition, the Raman peak located at 640 cm^{-1} can be attributed to Mn-O vibrations, revealing the presence of MnO_2. X-ray photoelectron spectroscopy (XPS) was used to estimate the various chemical states of the bonded elements. As shown in Figs. 3b-d, the Mn 2p XPS spectrum shows two major peaks centered at approximately 654.2 eV and 642.6 eV, corresponding to Mn 2p1/2 and Mn 2p3/2, respectively. The characteristic of the MnO_2 phase with a spin-energy separation of 11.6 eV coincides with a previous report. [19] Additionally, the XPS spectrum of C 1s shows three signals of C-C (284.6 eV), C-O (286.7 eV) and O-C=O (288.6 eV), which are possibly from the covalent oxygen groups on the graphene (Fig. 3d).

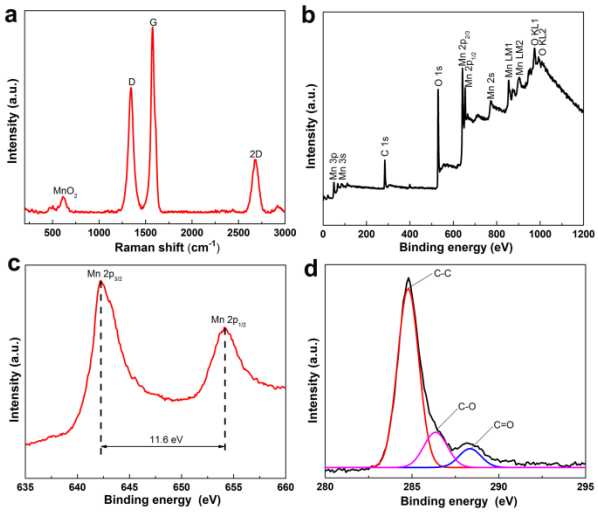

Figure 3. (a) Raman pattern and (b-d) XPS spectra of the MnO_2/graphene samples.

The morphologies of the MnO_2/graphene composites were further examined by scanning electron microscopy (SEM). Figs. 4a and b show representative SEM images of MnO_2/graphene with a highly porous nanostructure, which is composed of dense MnO_2 nanosheets with a thickness of ~10 nm. The MnO_2 nanosheets are homogeneously and tightly anchored onto the graphene surfaces. There is no collapse of the Ni foam struts or obstruction of the pores, indicating the strong mechanical strength of the MnO_2/graphene and the uniform dispersion of the MnO_2 nanosheets.

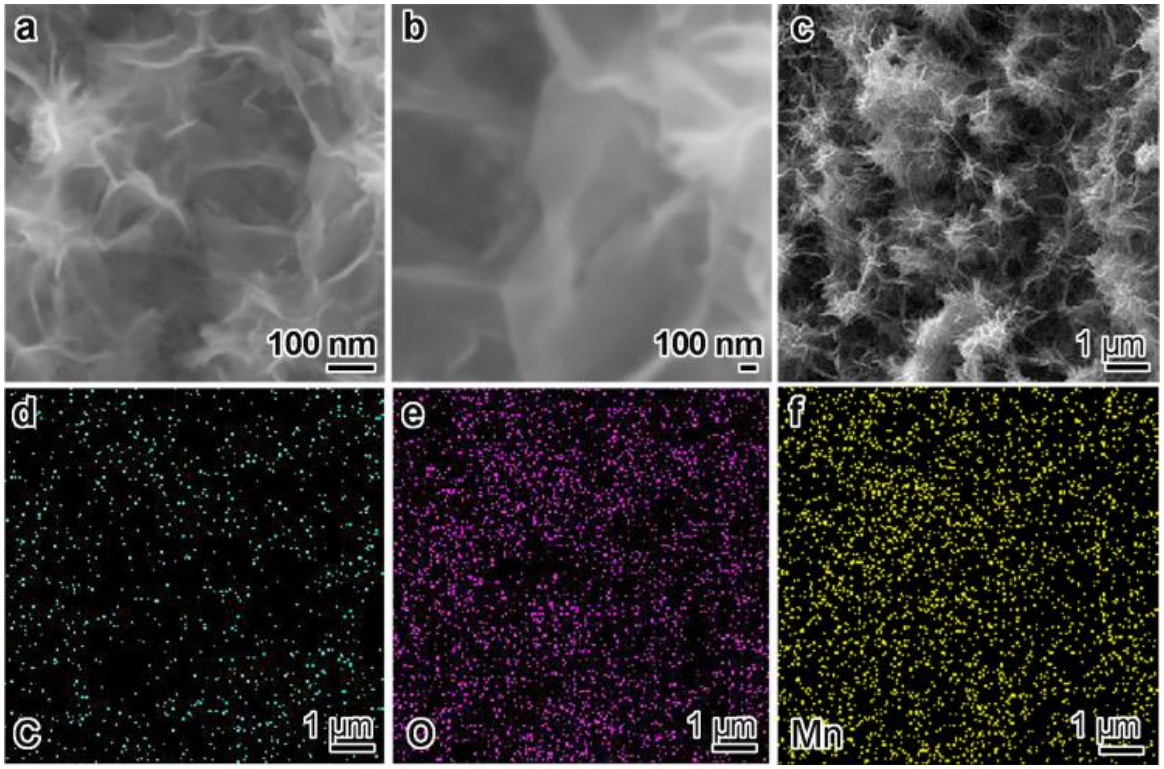

Figure 4. (a, b) SEM images of the MnO_2/graphene composites; (c) SEM images and corresponding EDS elemental mapping images of (d) C, (e) O and (f) Mn.

Table 1. Element composition of the MnO_2/graphene composites.

Element	Wt.%	Atom %
C	5.12	7.91
O	24.16	50.00
Mn	57.14	34.44
Ni	13.57	7.65
Total	100.00	100.00

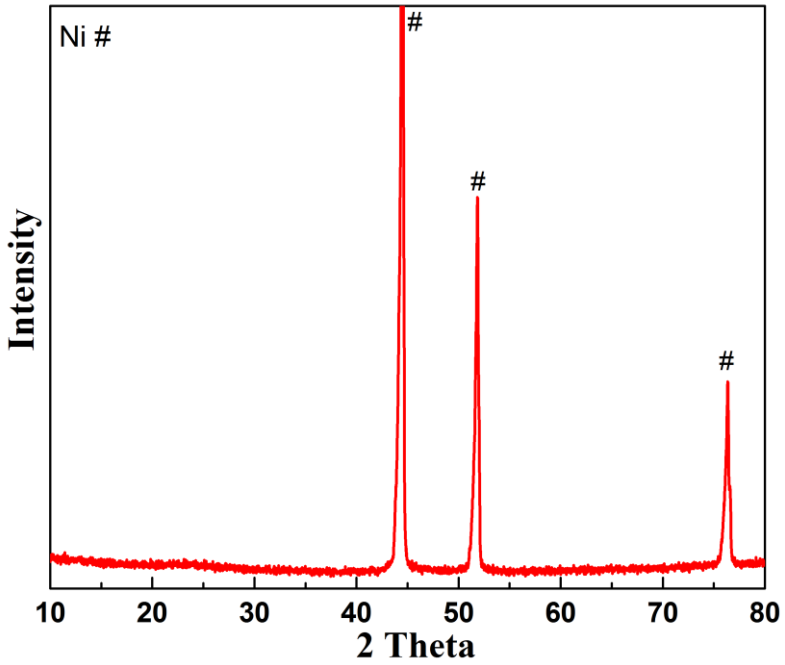

Figure 5. X-ray diffraction (XRD) measurement of the MnO_2/graphene composites.

Furthermore, the elemental mappings of C, O and Mn were investigated from a square region on the foam (Figs. 4c-f), suggesting a continuous, uniform distribution of MnO_2 and graphene on the 3D Ni foam surfaces. The corresponding EDS mapping also revealed that the C element content of the MnO_2/graphene composites is approximately 7.91 % (atomic ratio, Table 1). In addition, except for the peaks associated with the Ni foam substrate, no other peaks are present in the X-ray diffraction pattern of the MnO_2/graphene (Fig. 5), which further confirms its amorphous structure.

Table 2 Specific capacitance and retention of the supercapacitors based on MnO_2/graphene at a current density of 1 A/g

Samples	Specific capacitance ($F\ g^{-1}$)	Capacitance retention (%- cycles)	Reference
MnO_2/graphene	158	83.4-5,000	[21]
MnO_2/graphene	280	99-1,0000	[22]
MnO_2/graphene	306	95.2-5,000	[23]
MnO_2/graphene	324	96.8-1,000	[24]
MnO_2/graphene	350	93-5,000	[25]
MnO_2/graphene	358	80-1,000	[26]
MnO_2/graphene	476	-	[27]
MnO_2/graphene	***607***	***94-1,0000***	***This work***
MnO_2/graphene	***607***	***94-1,0000***	***This work***

In view of its unique structure and morphology, the as-prepared MnO_2/graphene composites were expected to possess excellent electrochemical performance for a supercapacitor. The performance of MnO_2/graphene composites was further evaluated in a three-electrode test cell. Figure 6a presents current-voltage (CV) curves of the MnO_2/graphene composites in a 1 M Na_2SO_4 electrolyte at different scan rates from 0.0 to 0.8 V. The CV scans exhibited rectangular shapes and symmetry, indicating their ideal pseudocapacitive behavior. The specific capacitances were 607, 482, 214, and 171 F g^{-1} at current densities of 1, 2, 4 and 8 A g^{-1}, respectively, calculated by the formula of $C = I\Delta t/(\Delta Vm)$[20]. Here, I, Δt, m and ΔV correspond to the discharge current, time, the mass of the active materials and the potential change during discharge, respectively.

As shown in Figure 6a, the specific capacitance gradually decreased with increasing current density. Notably, the specific capacitance of the samples reached 607 F g^{-1} at 1 A g^{-1}, exceeding the common MnO_2/graphene-based materials (Table 2). The uniform hybridization and coassembly between MnO_2 and high-quality graphene would ensure their high conductivity and good pseudocapacitive properties thus contributing to their remarkable capacitance. The Nyquist plot in Figure 6c shows a resistance of 3.2 Ω of the device, revealing the high conductivity of the samples. Moreover, the 3D porous structure of MnO_2/graphene can effectively facilitate electrolyte diffusion and propagation of electrons, enabling the high specific capacitance of the MnO_2/graphene composites.

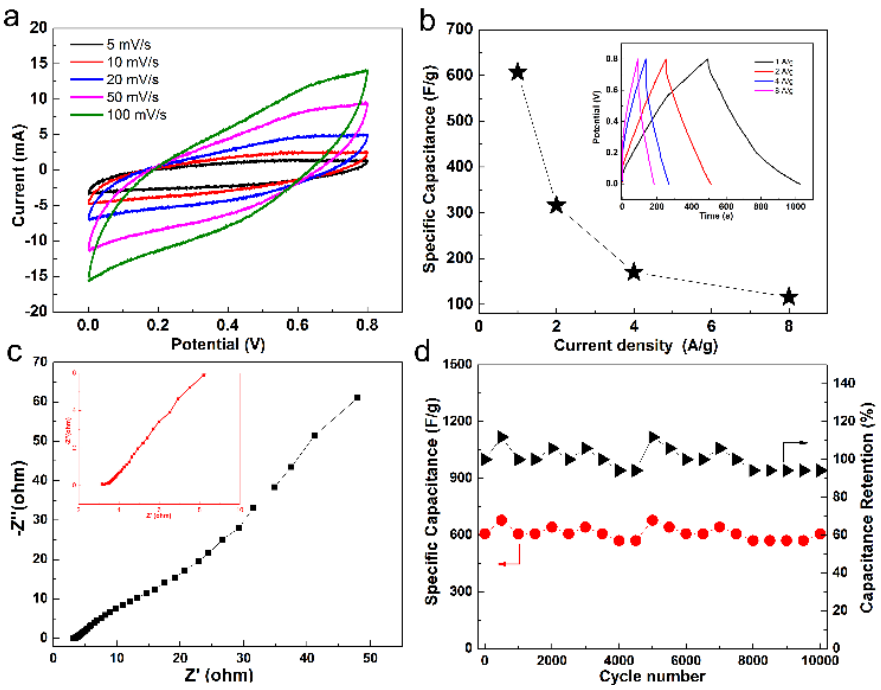

Figure 6. Electrochemical performance of the MnO_2/graphene composite. (a) CV curves at different scan rates; (b) Gravimetric specific capacitance of MnO_2/graphene composite as a function of the current densities (the inset illustrates galvanostatic charging/discharging curves at various current densities); (c) Nyquist plot of the MnO_2/graphene composite; and (d) Cycling performance of MnO_2/graphene composite at 1 A g^{-1}.

Figure 6d shows that the 3D MnO_2/graphene composite supercapacitor exhibited outstanding cycling stability at a current density of 1 A g^{-1}. The retention can reach 94 % of the initial capacitance even after 10000 cycles. By comparison, the MnO_2 film without graphene only retained 24.4 % of the initial capacitance after 2000 cycles (Figure 7). These results highlighted the significant role of the hybrid interface between MnO_2/graphene in electron transport.

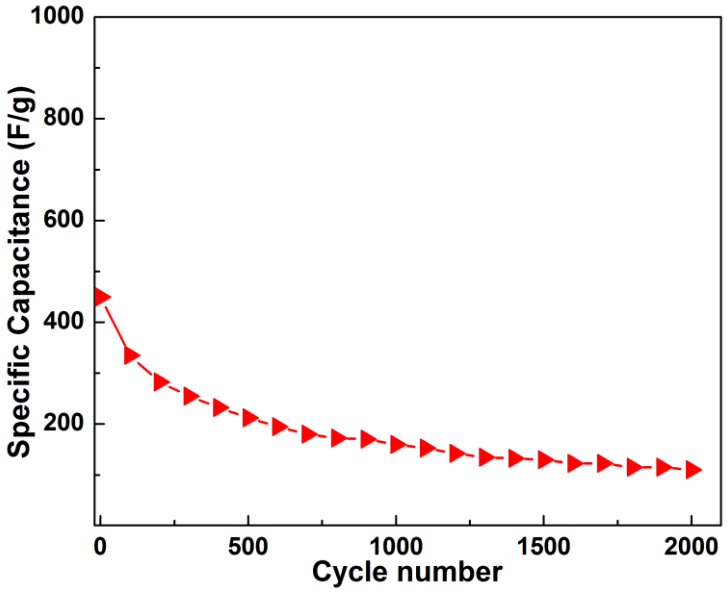

Figure 7. Cycling performance of MnO_2 without graphene at 1 A/g.

4. CONCLUSIONS

In conclusion, we demonstrate a one-step electrochemical approach to cooperatively grow and assemble MnO_2 and graphene on 3D Ni foam. The electrochemical-assisted hybridization of MnO_2 nanosheets with high-quality graphene as well as the unique architecture of the 3D skeleton provided MnO_2/graphene composites with high conductivity, ion diffusivity and capability to accommodate volume changes during faradaic reactions. As a result, the as-prepared 3D MnO_2/graphene composites possess high specific capacitance (607 F g^{-1}), remarkable rate capability and superlong cycle life (94 %, after 10,000 continuous charge-discharge cycles) when used as electrode materials for supercapacitors. Our study provides new insight into the facile fabrication of multicomponent hybrids towards high-performance energy storage devices.

CONFLICT OF INTEREST
None.

ACKNOWLEDGEMENT
We thank the Natural Science Foundation of China (Grant No. 11174197, 11574203, 61234005 and 51773062) for its support.

References

1. L. L. Zhang, X. Zhao, *Chem. Soc. Rev*., 38 (2009) 2520-2531.
2. C. Cui, J. Xu, L. Wang, D. Guo, M. Mao, J. Ma, T. Wang, *ACS Appl. Mater. Inter.*, 8 (2016) 8568-8575.
3. N.A. Kyerematen, T. Brousse, D. Pech, *Nature Nanotech*., 12 (2017) 7-15.
4. H.-S. Kim, J.B. Cook, H. Lin, J.S. Ko, S.H. Tolbert, V. Ozolins, B. Dunn, *Nature Mater.*, 16 (2017) 454-460.
5. M. Salanne, B. Rotenberg, K. Naoi, K. Kaneko, P.-L. Taberna, C. Grey, B. Dunn, P. Simon, *Nature Energy,* 1 (2016) 16070.
6. W. Gao, N. Singh, L. Song, Z. Liu, A.L.M. Reddy, L. Ci, R. Vajtai, Q. Zhang, B. Wei, P.M. Ajayan, *Nature Nano.*, 6 (2011) 496-500.
7. M. Toupin, T. Brousse, D. Bélanger, *Chem. Mater.*, 14 (2002) 3946-3952.
8. K. Shimamoto, K. Tadanaga, M. Tatsumisago, *Electrochim. Acta.*, 109 (2013) 651-655.
9. H. Ye, Y. Cheng, T. Hobson, L. Jie, *Nano Lett.*, 10 (2010) 2727-2733.
10. T. Brousse, P.L. Taberna, O. Crosnier, R. Dugas, P. Guillemet, Y. Scudeller, Y. Zhou, F. Favier, D. Bélanger, P. Simon, *J. Power Sources,* 173 (2007) 633-641.
11. C. Chen, W. Fu, C. Yu, *Mater. Lett*., 82 (2012) 133-136.
12. N. Gao, X. Fang, *Chem. Rev.*, 115 (2015) 8294-8343.
13. Z. Li, S. Gadipelli, Y. Yang, Z. Guo, *Small,* 13 (2017) 1702474
14. Y. Zhao, L. Hu, S. Zhao, L. Wu, *Adv. Funct. Mater*., 26 (2016) 4085-4093.
15. Z. Li, Y. An, Z. Hu, N. An, Y. Zhang, B. Guo, Z. Zhang, Y. Yang, H. Wu, *J. Mater. Chem*. *A*, 4 (2016) 10618-10626.
16. L. Qian, L. Lu, *Colloids & Surfaces A*, 465 (2015) 32-38.
17. L. Peng, P. Xu, B. Liu, C. Wu, Y. Xie, G. Yu, *Nano Lett.*, 13 (2013) 2151-2157.
18. L. Ma, M. Zheng, S. Liu, Q. Li, Y. You, F. Wang, L. Ma, W. Shen, *Chem. Commun.,* 52 (2016) 13373-13376.
19. S. Chen, J. Zhu, X. Wu, Q. Han, X. Wang, *Acs Nano*, 4 (2010) 2822-2830.
20. M. Jin, G. Zhang, F. Yu, W. Li, W. Lu, H. Huang, *Phys. Chem. Chem. Phys*., 15 (2013) 1601-1605.
21. H. Gao, F. Xiao, C.B. Ching, H. Duan, *Acs Appl. Mater. & Inter.,* 4(5) (2012) 2801-10.
22. Z. Li, Y. An, Z. Hu, N. An, Y. Zhang, B. Guo, Z. Zhang, Y. Yang, h. Wu, *J. Mater. Chem. A,* (2016).
23. L. Li, R. Li, S. Gai, S. Ding, F. He, M. Zhang, P. Yang, *Chem.-Eur. J.* 21(19) (2015) 7119-26.
24. Q. Yong, S. Lu, F. Gao, *J. Mater. Sci.,* 46(10) (2011) 3517-3522.
25. H. Huang, G. Sun, J. Hu, T. Jiao, *J. Chem.,* 2015 (2015) 1-8.
26. L. Qian, L. Lu, *Colloids & Surfaces A*, 465 (2015) 32-38.
27. Y.Q. Zhao, D.D. Zhao, P.Y. Tang, Y.M. Wang, C.L. Xu, H.L. Li, *Mater. Lett.*, 76(6) (2012) 127-130.